Three Level Inverter based DTC of Induction Motors Utilizing RCPWM

Monika Abrol, Shweta Singh, Mukesh Kumar and Kuldeep Singh Kulhar

Dr. Monika Abrol, Dean, Department of Applied Science, Sanskriti University, Mathura, Uttar Pradesh, India, Email Id -dean.shss@sanskriti.edu.in
Shweta Singh , Assistant Professor, Maharishi School of Engineering & Technology, Maharishi University of Information Technology, Uttar Pradesh, India, Email Id-shwetasingh580@gmail.com
Mukesh Kumar, Assistant Professor, Mechanical Engineering, Vivekananda Global University, Jaipur, India, Email Id-kumar.mukesh@vgu.ac.in
Kuldeep Singh Kulhar, Professor, Civil Engineering, Vivekananda Global University, Jaipur, India, Email Id-k.singh@vgu.ac.in

Abstract— **This paper introduces a streamlined space vector algorithm designed to regulate a three-level inverter-powered induction motor using direct torque control (DTC). Unlike the traditional two-level inverter, this drive utilizes a three-level inverter to achieve a reduction in torque ripple. The controller has been specifically designed to capitalize on the expanded range of inverter states that are made possible by utilizing a three-level inverter. The algorithm proposed in this study is flexible and can be applied to various rail clamping pulse width modulation (RCPWM) sequences. The RCPWM-3 demonstrates superior performance, which enhances the drive's performance at near rated speeds. The findings indicate a reduction in harmonic distortion within the stator currents, alongside a consistent switching frequency of the inverter through the implementation of the suggested control system.**

Index Terms—**DTC, Induction motor, 3-level inverter, SVM, speed control.**

Corresponding Author: dean.shss@sanskriti.edu.in

1. INTRODUCTION

The conventional two-level VSI is frequently utilized in electrical drive systems, yet it comes with particular limitations. The maximum voltage capacity of the semiconductor switching devices in the VSI is a constraint that limits the peak value of the DC link voltage. Furthermore, the output voltages and currents of the VSI demonstrate notable levels of harmonic distortion. Additionally, the voltage waveforms at the output could exhibit higher dV/dt values, resulting in the degradation of the insulation and bearings of the machine, as well as significant electromagnetic interference while in operation. However, by utilizing multilevel VSI topologies, many of these limitations can be overcome. The three-level neutral point clamped (NPC) VSI is widely used among the different multilevel inverter (MLI) topologies. This specific iteration of VSI provides numerous benefits when compared to the conventional two-level VSI. The benefits include a higher number of levels in the output voltage waveforms, reduced harmonic distortion, and lower switching frequencies [1-2].

In recent years, induction motor control has gained significant attention in various applications that utilize automated machines. This increased focus can be attributed to advancements in the field of power electronics. Field-oriented control, a technique that allows an AC motor to achieve dynamic responses comparable to those of a DC motor, has been developed [3-4],[5-8]. This control strategy is based on regulating the stator current. Numerous researchers have dedicated their efforts to addressing the challenges associated with this control method. However, an alternative to field-oriented control, known as direct torque control (DTC), has emerged [8-10]. Despite extensive research on two-level topologies in relation to DTC, there has been limited investigation into DTC systems employing multilevel topologies. The three-level voltage source inverter (VSI) topology offers a significant advantage when applied to DTC. It provides a greater number of voltage vectors, resulting in a more precise control system that reduces torque and flux ripples. Nevertheless, this benefit is accompanied by a rise in intricacy during the selection of vectors. Several researchers have suggested utilizing DTC with more advanced topologies, yet their methods hinge on intricate vector selection tables and modulation techniques dependent on parameters [10-11]. An alternative approach involves the use of selection tables based on virtual vectors [12-13]. The methods discussed in this paper improve the control strategy, but they are more intricate compared to the traditional DTC system [8]. Furthermore, they do not lend themselves well to different multilevel topologies with a greater number of levels, as indicated in references [17-18], because of the particular table selection method that is employed. The paper introduces a reference voltage vector calculator (RVVC) based DTC that is compatible with different SVPWM methods. This approach eliminates the need for look-up tables and hysteresis comparators, and it is independent of the motor model in the control system, except for the inherent estimator that resembles the conventional DTC (CDTC) system.

This document presents RCPWM techniques for generating the stator voltage of an induction motor in order to achieve synchronized control of torque and stator flux. The utilization of a clamped neutral point three-level inverter, as depicted in Figure 1, allows for the application of instantaneous voltage vectors with redundancy characteristics. This redundancy provides flexibility in selecting the inverter switching modes. The control system attains several objectives by utilizing this switching freedom: regulation of the primary flux, high-speed torque control, and reduction of the inverter switching frequency. The machine's dynamic performance is significantly enhanced when compared to conventional speed control methods for induction motor drives, resulting in improved outcomes. In order to verify these findings, a simulation program has been created.

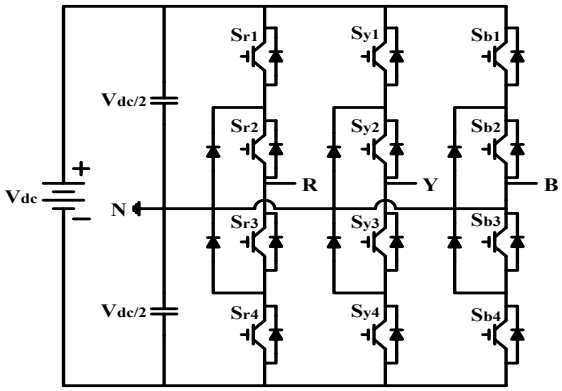

Fig. 1 3-phase 3-level NPC.

2. SPACE VECTOR TECHNIQUE

The averaging process is used to form the reference vector in the space vector approach to PWM. The switching cycle lasts for a time period of T_s, and an average vector, V_{ref}, is produced to uphold the volt-second balance principle. The inverter utilizes the nearest voltage vectors in each switching cycle by averaging their corresponding voltage vectors. The voltage vectors and their corresponding switching states are shown on a three-level α-β axis space plane, as demonstrated in Figure 2.

For the conventional two-level inverter, the nearest switching states for the same position and magnitude of V_{ref} are V0, V1, V2, and V0, as depicted in Figure 3. However, with the three-level inverter, there are additional switching states available, which can further reduce voltage ripple. The closest switching states to the three-level inverter are V7, V1, V13, and V7. Additionally, the three-level inverter has additional switching states, namely V7, V8, V9, V10, V11, and V12.

Table I illustrates the switching states and inverter switch positions for the r-phase.

Table I Switching pattern.

Switching patterns	ON states	Voltage
2	S_{r1} & S_{r2}	$V_{dc}/2$
1	S_{r2} & S_{r3}	0
0	S_{r3} & S_{r4}	$-V_{dc}/2$

The proposed algorithm maintains the same number of steps needed to synthesize the V_{ref} using a three-level inverter as compared to a two-level inverter. Nevertheless, there is a change in the starting point of V_{ref}, which now aligns with the center of the sub hexagon where V'_{ref} is positioned, as illustrated in Figure 3. The newly shifted reference vector, V'_{ref}, has a starting point of 100 and forms an angle β with respect to the α axis. The durations for which the large voltage vector state 1 (200), another large voltage vector state 2 (210), and the two middle voltage vector states (100, 211) need to be applied are determined by T1, T2, and Tz, respectively. These durations are given by equations (1)-(3). In these equations, 'M' represents the modulation index.

$$T_1 = M * \frac{Sin(60^0 - \beta)}{Sin60^0} * T_s \quad (1)$$

$$T_2 = M * \frac{Sin(\beta)}{Sin(60^0)} * T_s \quad (2)$$

$$T_Z = T_s - T_1 - T_2 \quad (3)$$

The allocation of time between the two zero states is a design parameter that provides flexibility in the development of PWM strategies in the space vector domain [13-14]. Figure 4 illustrates the distribution of active state and zero state duration for the 0127, 012, and 721 sequences. Typically, an equal division of time results in reduced ripple current [13] at low modulation indices. The sequence 0127, which evenly distributes time between the zero states, is commonly employed in conventional space vector modulation (CSVPWM) to produce specific samples within sector-I.

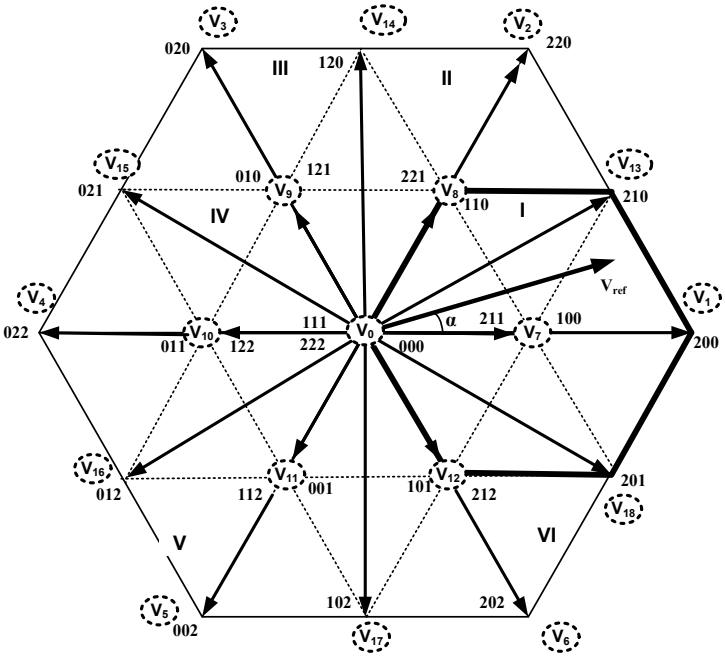

Fig.2. Space Vector for 3-phase 3-level.

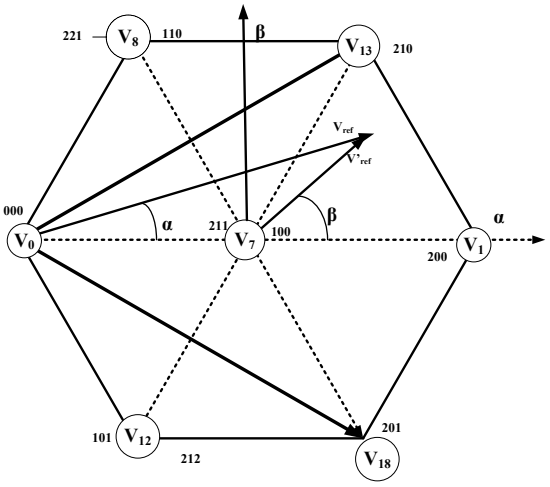

Fig. 3 Shifting reference vectors.

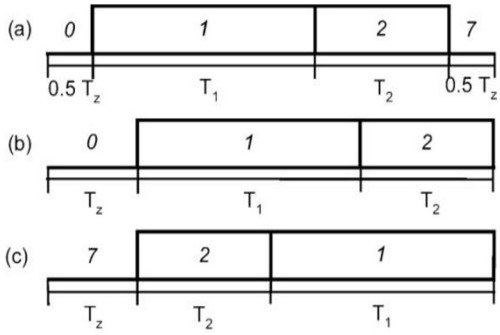

Fig. 4 CSVPWM and RCPWM sequences.

Sequences such as 012 or 721, which only utilize a single zero state, can also be employed to produce the same sample. By utilizing these sequences in a slightly higher modulation region, the current ripple can be reduced [14-15]. Additionally, it is possible to decrease the current ripple in higher modulation regions by using the sequences 012, 721, 2721, or 1012 to produce the sample, splitting one of the active state or into two equal intervals [14-17]. The division of switching time and placement of switching states with 0127, 012, and 721 are illustrated in Figure 4. The RCPWM methods generated using the 012 and 721 sequences are referred to as RCPWM-1 to RCPWM-6. One of the phases is clamped to either the positive rail or the negative rail for 600 in every half cycle, continuously or discontinuously, depending on the choice of the zero state and the instant of varying the zero state. Based on these criteria, various RCPWM methods can be generated. The zero state used and the position of zero state switching are depicted in Figure 5. The modulating waveforms and zero sequence signals of the considered RCPWM methods are shown in Figure 6. In the CSVPWM method, the modulating waves do not clamp to the DC rail, resulting in the generation of continuous pulses and making this PWM a continuous PWM method. The diagram related to this is displayed in Figure 7. The switching pulses for the CSVPWM sequence 0127 for all three phases are shown in Figure 8. The execution of the sequences in Sector-I is tabulated in Table II. In the case of RCPWM-3 to RCPWM-6 methods, the sequences shown should reverse in even sectors.

Table II Sequences to be executed in Sector-I (odd) and Sector-II (even)

PWM Method	$0^0 \le \alpha \le 30^0$	$30^0 \le \alpha \le 60^0$	$0^0 \le \alpha \le 30^0$	$30^0 \le \alpha \le 60^0$
RCPWM-1	721	721	721	721
RCPWM-2	012	012	012	012
RCPWM-3	721	012	012	721
RCPWM-4	721	721	721	721
RCPWM-5	012	721	721	012
RCPWM-6	012	012	012	012

Table III Possible Switching sequences for subsectors of Hexagon -1

Sub sector	Switching sequence

1	100-200-210-211or 100-200-210 or 211-210-200
2	100-110-210-211or 100-110-210 or 211-210-110
3	100-110-111-211or 100-110-111 or 211-111-110
4	100-101-111-211or 100-101-111 or 211-111-101
5	100-101-201-211 or 100-101-201 or 211-201--101
6	100-200-201-211 or 100-200-201 or 211-201-200

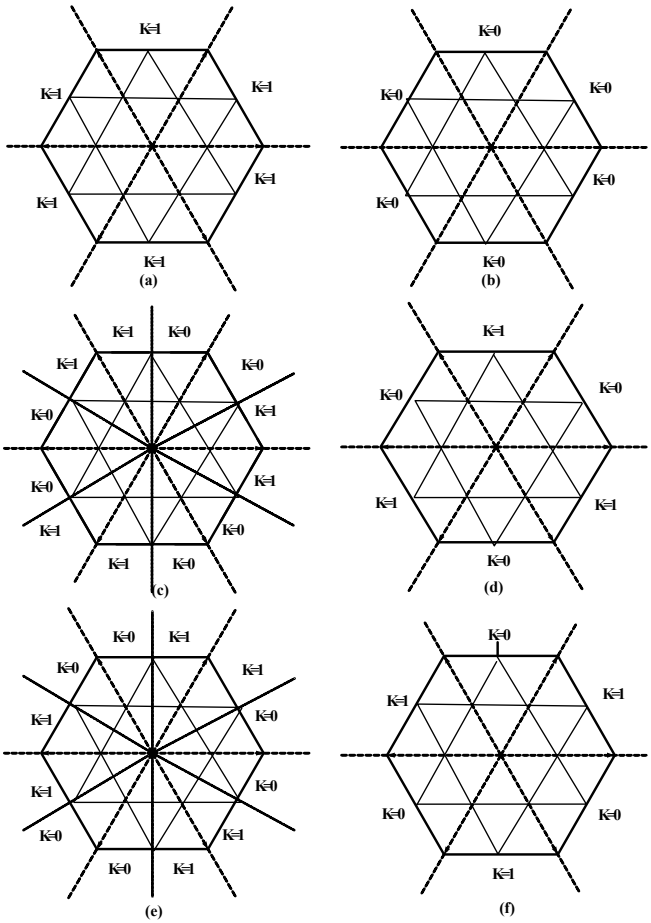

Fig. 5 Schematic diagrams showing the instant of variation of k to generate various RCPWM methods (a) RCPWM-1 (b) RCPWM-2 (c) RCPWM-3 (d) RCPWM-4 e) RCPWM-5 (f) RCPWM-6

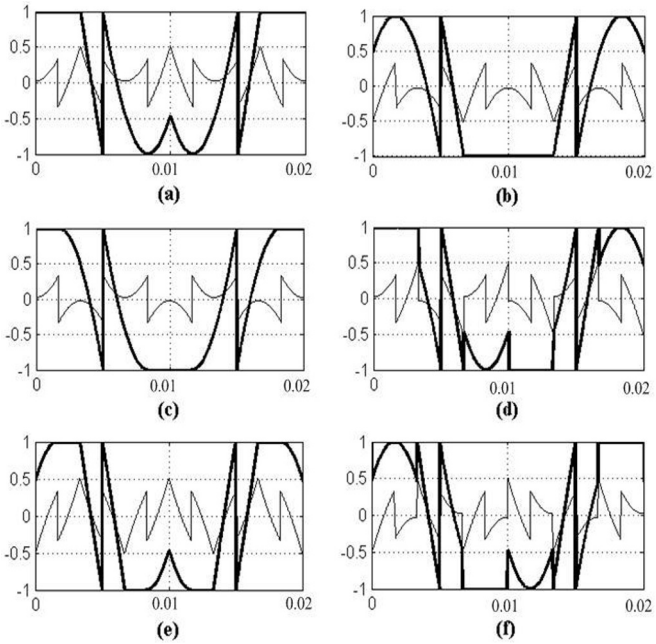

Fig.6. Modulation waveforms and zero sequence signals of some popular existing RCPWM methods: (a) RCPWM-1 (b) RCPWM-2.
(c) RCPWM-3 (d) RCPWM-4 e) RCPWM-5 (f) RCPWM-6.

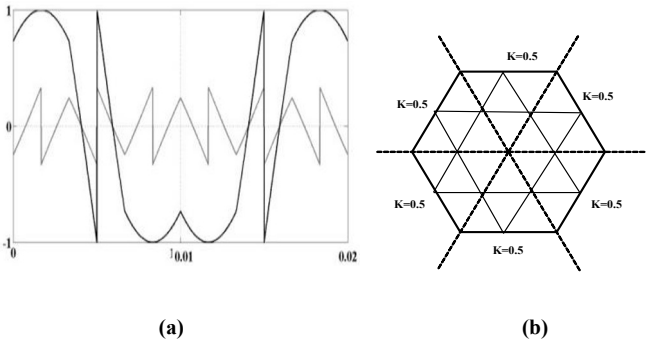

Fig. 7. Modulating waveform and zero sequence signal of CSVPWM method.

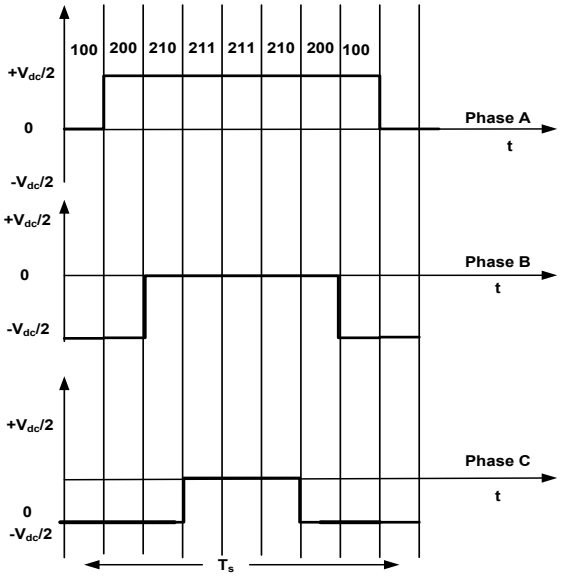

Fig. 8 Switching pulses with CSVPWM sequence (0127).

3. EXTENSION OF SPACE VECTOR APPROACH TO RCPWM GENERATION

With The space vector approach allows for the easy generation of different PWM methods by simply changing the value of 'k'. The focus of this study is on a new approach for generating 'k', where only the instantaneous values of two sets of phase voltages are used to generate different RCPWM methods. This paper proposes a generalized procedure, using a constant variable 'k', through which all considered RCPWM methods can be generated. This algorithm is referred to as the generalized RCPWM (GRCPWM) algorithm. The value of 'k' determines the type of RCPWM method by controlling the zero state times. The division of zero state times with the aid of 'k' is illustrated in Figure 5. In the CSVPWM method, the modulating wave does not clamp to the DC rail, resulting in the generation of continuous pulses and making it a continuous PWM method. This is in contrast to RCPWM methods, where the modulating waveform clamps to either of the rails for 1200 in each cycle.

$T_0 = (1-k)T_z ; T_0 = kT_z$ **Ошибка! Источник ссылки не найден.** (4)

$$V_i = V_{ref} \cos(\theta - 2(r-1)\frac{\pi}{3}) \quad (5)$$

Ошибка! Источник ссылки не найден. $V_{ix} = V_{ref} \cos(\theta - 2(r-1)\frac{\pi}{3} - \frac{\pi}{6})$ (6)

for r= 1, 2, 3 & i = a, b, c.

The duration of the active and zero states can be determined by utilizing the instantaneous phase voltages and are provided in (6).

$T_1 = \left[\frac{T_s}{V_{dc}}\right](v_{\max} - v_{\min})$ **Ошибка! Источник ссылки не найден.** (7)

Ошибка! Источник ссылки не найден. $T_2 = \left[\frac{T_s}{V_{dc}}\right](v_{mid} - v_{\min})$ (8)

$T_Z = T_S - T_1 - T_2$ **Ошибка! Источник ссылки не найден.** (9)

At a given sampling instant, V_{max}, V_{min}, and V_{mid} represent the maximum, minimum, and non-maximum or minimum values of V_{in}. The proposed GRCPWM algorithm allows for the generation of various PWM methods by adjusting the zero voltage vector time distribution parameter k between 0 and 1. Table IV displays the different PWM methods obtained by varying the k value. Additionally, Fig. 8 illustrates the pattern of the switching pulses for the three phases in a CSVPWM sequence. Due to the symmetrical nature of the switching pulses, it is also known as a symmetrical sequence.

Table IV Various PWM methods by varying the value of k.

RCPWM Methods	Value of k
CSVPWM	0.5.
RCPWM-1	1.
RCPWM-2	0.
RCPWM-3	If $V_{max} + V_{min} < 0$ then k=0. If $V_{max} + V_{min} \geq 0$ then k=1.
RCPWM-4	If $V_{max,x} + V_{min,x} < 0$ then k=0. If $V_{max,x} + V_{min,x} \geq 0$ then k=1.
RCPWM-5	If $V_{max} + V_{min} < 0$ then k=1. If $V_{max} + V_{min} \geq 0$ then k=0.
RCPWM-6	If $V_{max,x} + V_{min,x} < 0$ then k=1. If $V_{max,x} + V_{min,x} \geq 0$ then k=0.

To generate CSVPWM pulses through space vector approach implemented by GRCPWM algorithm, in all sectors of the space plane in which V_{ref} lies, k takes 0.5. Similarly, for k equals to 0 and 1 pulses same as that generated by comparing the modulating waveforms shown in Fig. 6(a) and Fig. 6(b) with a triangular wave could be generated. These two space vector based PWM methods are referred as RCPWM-1 and RCPWM-2 respectively. But for generating RCPWM-3 and RCPWM-6 pulses, the odd and even sectors need to be distinguished for keeping k equals to 0 and 1 respectively. So to distinguish odd/even sectors three phase reference voltage waveforms V_a, V_b, V_c are phase shifted by 30^0 to get V_{ax}, V_{bx}, V_{cx} as shown in Fig. 9. Using the logic shown in Table II, this can be done to synthesize space vector pulses similar to that by comparing the modulating waveforms shown in Fig. 6(d) and Fig. 6(f) with a high frequency carrier wave. To generate RCPWM-3 and RCPWM-5 pulses in each odd and even sectors for $0^0 \leq \alpha \leq 30^0$ **Ошибка! Источник ссылки не найден.** k is made equal to 0 or 1 and for $30^0 \leq \alpha \leq 60^0$ **Ошибка! Источник ссылки не найден.** k is made equal to 1 or 0 respectively. For finding the instant at which the reference vector crosses the 30^0 angular position in each sector the instantaneous reference voltage components V_a, V_b, V_c are used as specified in Table IV.

Consider a switching instant AA' at which the reference voltage vector V_{ref} lies in sector-I as shown in Fig. 9. At this switching instant V_{max} is V_a , V_{min} is V_c and so V_{mid} is V_b. The condition $V_{max} + V_{min} \geq 0$ is satisfied up to $\theta=0^0$ to 30^0 and $V_{max} + V_{min} < 0$ satisfies for $\theta=30^0$ to 60^0. Hence implementing the logic shown in Table IV, k can be made to change from '0' to '1' without the need of reference vector position. Similarly implementing the logic specified in Table IV will generate other PWM methods. It is

observed that at this switching instant AA' the switching times become functions of line voltages, $T_1 = \left(\frac{T_s}{V_{dc}}\right)\left(v_{ac}\right)$ **Ошибка! Источник ссылки не найден.** and **Ошибка! Источник ссылки не найден.** . $T_2 = \left(\frac{T_s}{V_{dc}}\right)\left(v_{bc}\right)$

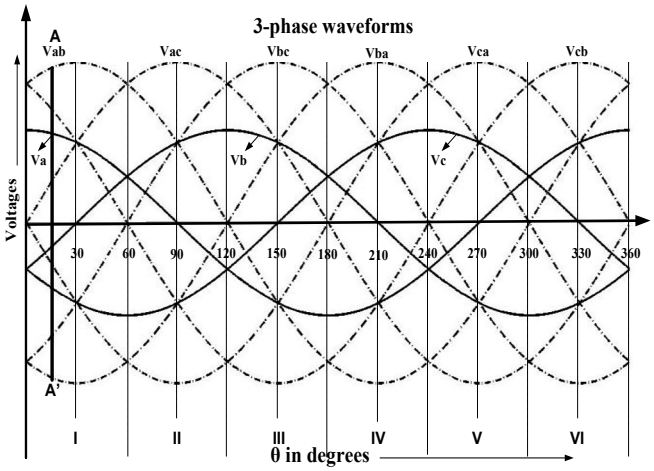

Fig. 9 Three phase and line votlage waveforms for online computation of FSTs.

4. NEED FOR DIRECT TORQUE CONTROL

In general applications, there is an increasing use of inverter-fed induction motors. A common and straightforward approach to regulate speed involves adjusting the input voltage to the motor with frequency in an open loop. This technique maintains a constant V/f ratio. In stable operating conditions, the air gap flux of the machine is intricately connected to the ratio of V/f. As the frequency nears zero at low speeds, the stator voltage magnitude decreases. The decrease in voltage is offset by the stator resistance. To uphold the rated air gap flux and full load torque at zero speed, an auxiliary voltage is introduced to counteract the decrease in stator resistance at low speeds. When the load torque rises during steady-state operation, the slip also increases within the stability threshold, ensuring a balance between the developed torque and the load torque. Nevertheless, fluctuations in the supply voltage to the inverter or an increase in stator resistance due to temperature changes can result in variations in the air gap flux. These fluctuations in air gap flux can cause alterations in torque sensitivity with slip frequency or stator current in a constant V/f control system. Failure to maintain the correct V/f ratio can result in a weakening or saturation of the air gap flux. A decrease in air gap flux will cause an increase in slip frequency for the same torque demand, ultimately leading to deterioration in the machine's response. Therefore, it is desirable to have a speed control scheme, such as DTC, that allows for independent control of torque and flux loop.

Historically, torque control in induction motors has typically been accomplished using FOC. This method involves converting the currents in the stator into a rotating d-q reference frame that aligns with the flux of the rotor. By segregating the torque and flux generating elements in this reference frame, a PI controller can be employed to manage the output voltage and attain the targeted stator current and torque. Nevertheless, the transient response of the torque controller is constrained by this PI controller.

On the other hand, DTC employs an induction motor model to achieve the desired torque output. It is possible to calculate the instantaneous stator flux and output torque by exclusively using current and voltage measurements. In order to achieve the desired flux and torque values within a specific time frame, a calculated voltage is predicted based on the induction motor model. This voltage is subsequently synthesized through SVM. The determination of the stator flux vector and the generated torque of the motor can be achieved by exclusively considering the voltage vector previously applied, the measured stator current, and the stator resistance.

5. PROPOSED GRCPWM BASED DTC

DTC, a widely used speed or torque control method in the VSI manufacturing industry, is recognized as a high-performance control strategy for AC drives [9-12]. Numerous authors have focused on enhancing the performance of DTC AC motors, particularly by reducing torque ripple and maintaining a constant switching frequency. Various approaches have been proposed [13]. However, extending these approaches to a higher number of levels is challenging, despite their suitability for the classical two-level inverter. This paper introduces GRCPWM based DTC as an efficient solution to mitigate these issues, with the added advantage of extending its application to MLIs. Many researchers have developed different approaches for multilevel inverters, as documented in [19-26]. However, this paper specifically discusses the three-level inverter. The block diagram of the CSVPWM based DTC can be seen in Fig. 10.

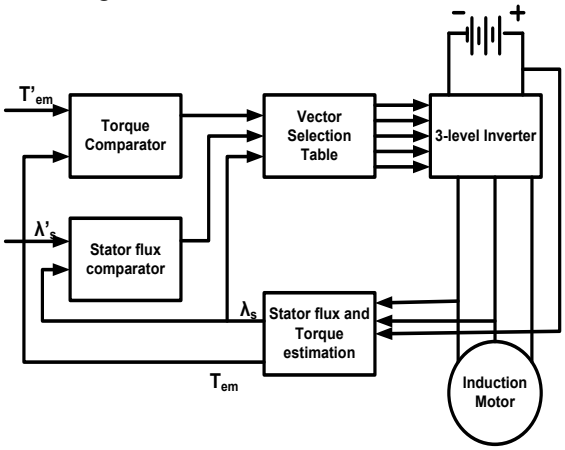

Fig. 10 Block diagram of three level CSVPWM based DTC.

In order to enhance the performance of the three level CSVPWM based DTC during high speed operations, a rail clamping based DTC has been developed using the GRCPWM algorithm. The block diagram of the proposed GRCPWM based DTC is illustrated in Figure 11. By implementing this three level algorithm, significant reductions in torque ripple, flux ripple, and current harmonic distortion can be achieved while maintaining a constant inverter switching frequency. The proposed DTC not only maintains all the benefits of the Conventional Direct Torque Control (CDTC), but also offers improved performance in regions with high modulation. The Carrier-SVPWM (CSVPWM) based DTC shows a limitation in this particular domain. The reference stator flux vector is produced by combining the slip speed with the actual speed from the adaptive motor model block. The reference d and q axis voltages are then calculated using equations (10)-(11) with the help of the reference voltage vector calculator. The magnitude and position of the reference voltage vector are then established based on these inputs. The GRCPWM block

employs a space vector technique to produce gating pulses for the inverter. The torque and speed of the adaptive motor model are determined by the voltages and currents of the d and q axes. The dynamic model of the induction motor is illustrated in the stationary reference frame according to reference [17].

$$V_{ds}^{*} = R_s i_{ds} + \frac{\Delta\psi_{ds}}{T_s} \tag{10}$$

$$V_{qs}^{*} = R_s i_{qs} + \frac{\Delta\psi_{qs}}{T_s} \tag{11}$$

where

$$\Delta\psi_{ds} = \psi_{ds}^{*} - \psi_{ds} \tag{12}$$

$$\Delta\psi_{qs} = \psi_{qs}^{*} - \psi_{qs} \tag{13}$$

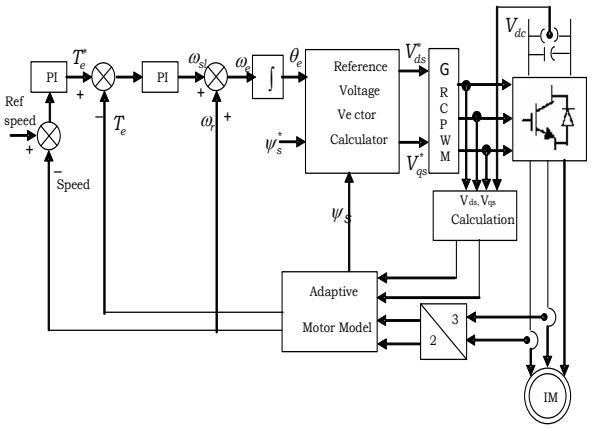

Fig. 11 Block diagram of three level GRCPWM based DTC.

6. RESULTS

In order to assess the effectiveness of the GRCPWM based DTC control on the three level inverter fed induction motor, a simulation was conducted using Matlab. The subsequent section presents the results obtained from this simulation. Figure 12 displays the trajectories of the locus traced by the direct axis flux in relation to the quadrature axis flux. Additionally, Figures 13 to 19 depict plots of steady state line currents, rotor speed, torque ripple, and flux magnitude with respect to simulation time for the six RCPWM methods considered. Other parameters of the system are considered from [27-28].

The analysis reveals a significant reduction in torque and flux ripple, as well as improved steady state performance in terms of speed and current distortion, when utilizing the RCPWM-3 method. Furthermore, Figure 20 illustrates the harmonic spectra (% of fundamental) for the three level inverter controlled with CSVPWM, RCPWM1, RCPWM2, RCPWM3, RCPWM4, RCPWM5, and RCPWM6 PWM methods, which were extended for DTC induction motor drive for speed control.

The findings indicate that when operating in high speed regions or during high modulation regions, RCPWM-3 exhibits superior harmonic spectra compared to the other PWM methods. This conclusion is supported by the simulation results. Therefore, it can be inferred that RCPWM-3 based DTC offers better performance for a three level inverter fed

induction motor. The simulation parameters used for this analysis are provided in the table below.

SIMULATION PARAMETERS.

Induction Motor details: 3-ϕ, 4-pole, 400V, 4.0kW, T=30.0N-m.

Resistance in Stator	1.571Ω.
Resistance in Rotor	1.210Ω.
Magnetizing Inductance	0.164H.
Inductance of Stator	0.172H.
Rotor inductance	0.172H.
Moment of Inertia	0.089Kg - m^2.
Viscous friction coefficient	0 N-m.sec/rad.

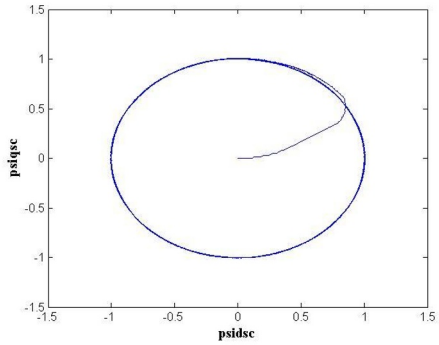

Fig.12a Three level CSVPWM based DTC : Locus of stator flux.

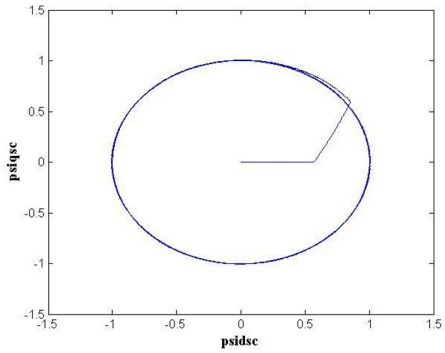

Fig.12b Three level RCPWM-3 based DTC: Locus of stator flux.

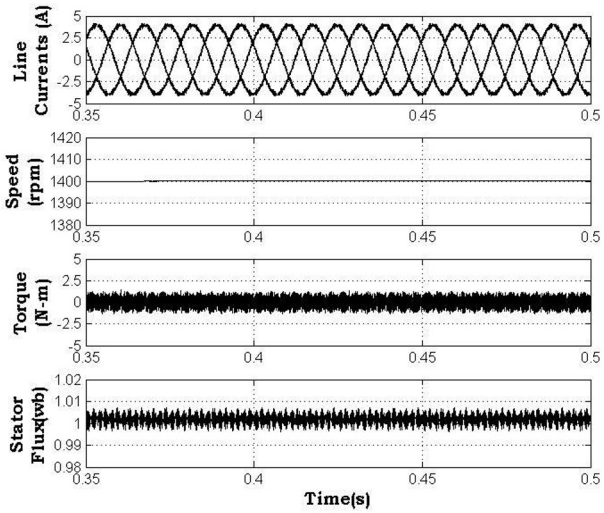

Fig.13. Steady state plots: Three level CSVPWM based DTC-3-level.

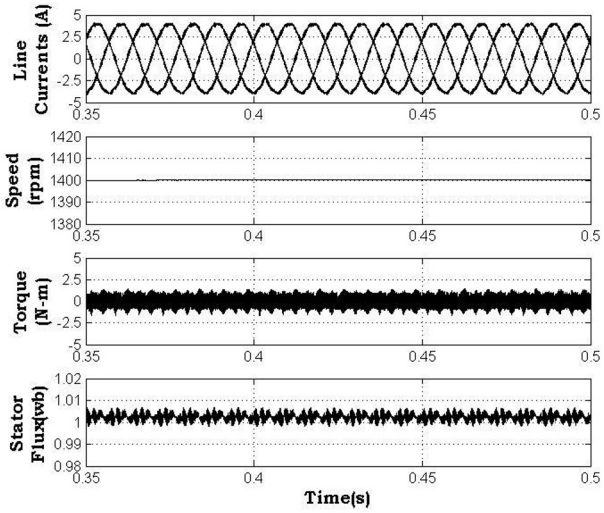

Fig.14. Steady state plots: Three level RCPWM-1 based DTC.

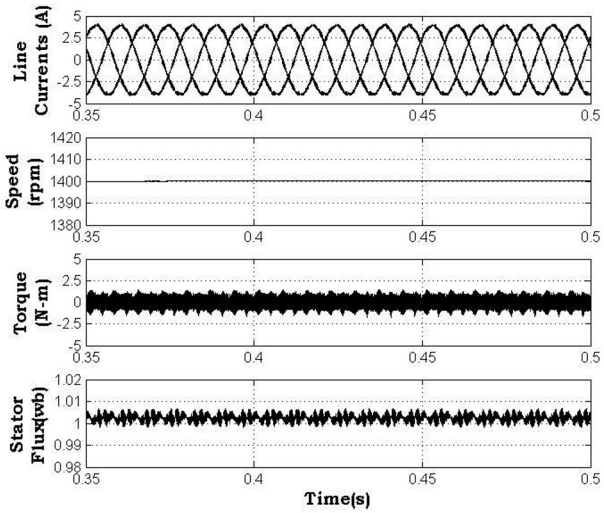

Fig.15 Steady state plots: Three level RCPWM-2 based DTC.

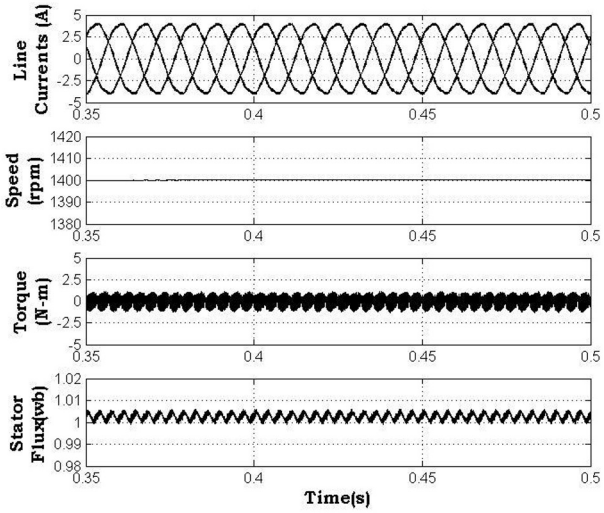

Fig.16. Steady state plots: Three level RCPWM-3 based DTC.

.

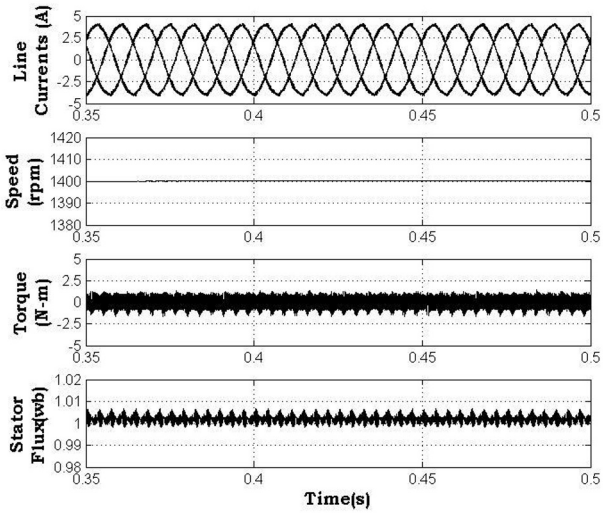

Fig.17. Steady state plots: Three level RCPWM-4 based DTC.

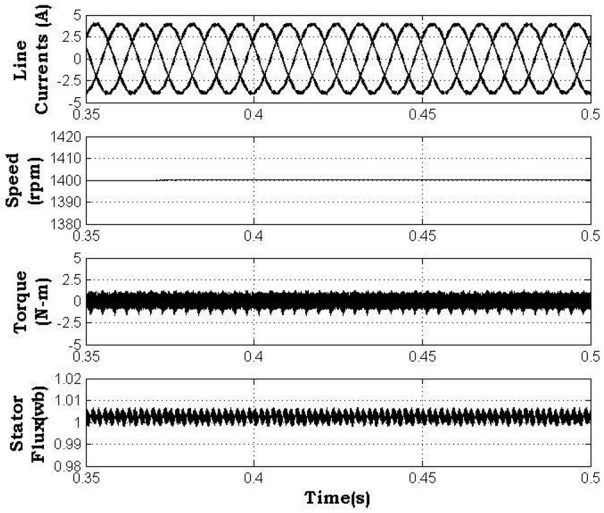

Fig.18. Steady state plots: Three level RCPWM-5 based DTC.

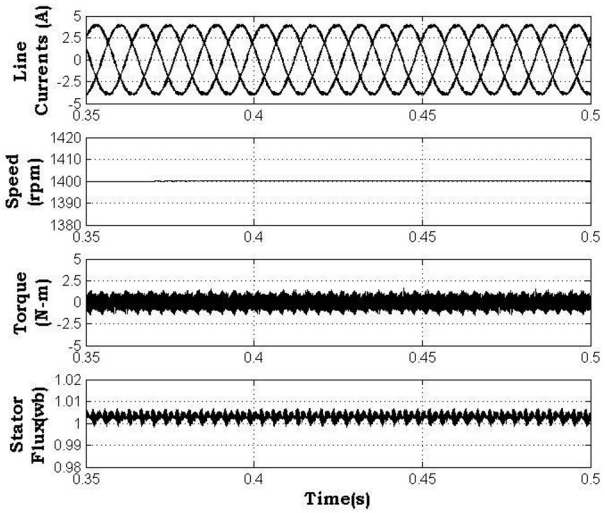

Fig.19. Steady state plots: Three level RCPWM-6 based DTC.

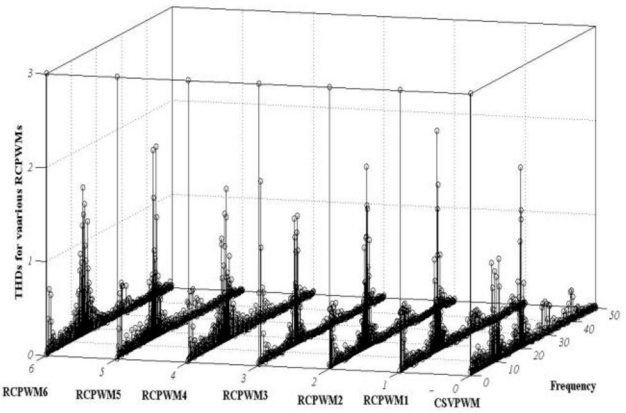

Fig.20 GRCPWM based DTC: Harmonic spectra (% of fundamental) comparison for CSVPWM, RCPWM-1, RCPWM-2, RCPWM-3 RCPWM-4, RCPWM-5, RCPWM-6.

THD Comparison table for various PWM

S.No	Various PWM Sequences	3-Level VSI Fed DTC IM
1	CSVPWM based DTC	4.75
2	RCPWM-1	4.69
3	RCPWM-2	4.69
4	**RCPWM-3**	**4.2**
5	RCPWM-4	4.49
6	RCPWM-5	4.73
7	RCPWM-6	4.50

7. CONCLUSIONS

The proposed DTC scheme utilizing a three-level VSI demonstrates significant improvements in various aspects compared to classical DTC systems using a two-level VSI. The enhancements encompass a significant decrease in torque fluctuation, flux fluctuation, distortion of harmonics in the switching frequency and stator currents. The direct torque control mechanism for a three-phase induction motor enables uninterrupted operation spanning from zero to maximum velocity. It has been proven that the computer program can accurately calculate the instantaneous primary flux, simplifying the data acquisition process. Furthermore, it has been demonstrated that through meticulous selection of zero state vectors and non-zero voltage vectors, in conjunction with their temporal duration, it is possible to regulate the magnitude of the electromagnetic torque. This facilitates independent manipulation of both flux and torque. In conclusion, the combination of a three-level inverter controlled by RCPWM-3 method with DTC speed control technique significantly enhances the overall efficiency of the drive when operating with high modulation.

REFERENCES

[1] U. R. Muduli, R. K. Behera, K. Al Hosani and M. S. E. Moursi, "Direct Torque Control With Constant Switching Frequency for Three-to-Five Phase Direct Matrix Converter Fed Five-Phase Induction Motor Drive," in IEEE Transactions on Power Electronics, vol. 37, no. 9, pp. 11019-11033, Sept. 2022, doi: 10.1109/TPEL.2022.3167477.

[2] U. R. Muduli, B. Chikondra and R. K. Behera, "Direct Torque Control of 3x5 Matrix Converter Fed Five-Phase IM Drive using Virtual Vector Concept," 2021 IEEE Applied Power Electronics Conference and Exposition (APEC), Phoenix, AZ, USA, 2021, pp. 765-770, doi: 10.1109/APEC42165.2021.9487140.

[3] Bimal K. Bose, “Modern power electronics and AC drives” Pearson Education, 2004.

[4] Peter Vas, “Sensorless vector and direct torque control” Oxford university press, New York, 1998.

[5] R. J. Lee, P. Pillay and R. G. Harley “D,Q Reference Frames for the Simulation of Induction Motors” *Electric Power Systems Research,* 8 (1984/85) pp.15 -26

[6] B. Mokrytzki, “Pulse width modulated inverters for AC motor drives" *IEEE Trans. on Ind. Gen. Appl*. Vol. IGA-3, No. 6, November/ December, 1967, pp. 493 - 503.

[7] F. Blaschke “The principle of field orientation as applied to the new transvector closed loop control system for rotating-field machines," *Siemens Review*, 1972, pp. 217-220.

[8] Isao Takahashi and Toshihiko Noguchi, “A new quick-response and high-efficiency control strategy of an induction motor,” *IEEE Trans. Ind. Applicat.*, vol. IA-22, no.5, Sep/Oct 1986, pp. 820-827.

[9] Domenico Casadei*,* Francesco Profumo*,* Giovanni Serra*,* and Angelo Tani, “FOC and DTC: Two Viable Schemes for Induction Motors Torque Control” *IEEE Trans. Power Electron.,* vol. 17, no.5, Sep, 2002, pp. 779-787.

[10] D. Casadei, G. Grandi, G. Serra and A. Tani, “Effects of Flux and Torque Hysteresis Band Amplitude in Direct Torque Control of Induction Machines” in *Proc.IECON’94,* Bologna, Italy, Sept.5-9, 1994, pp. 299-304.

[11] Jun-Koo Kang, Dae-Woong Chung and Seung-Ki Sul, “Direct torque control of induction machine with variable amplitude control of flux and torque hysteresis bands” in *Proc of the IEEE* EMD’99, 1999, pp. 640-642.

[12] G. Escobar, A.M. Stancivić, E. Galvan, J.M. Carrasco and R. Orgeta, "A family of switching control strategies for the reduction of torque ripple in DTC" *IEEE Trans. Control Systems Tech.,* vol. 11, no. 6, Nov 2003, pp. 933-939.
[13] Siva Ganesh Malla, "Modeling of 5-Phase Induction Motor: A Review", International Journal of New Technologies in Science and Engineering (IJNTSE), Vol. 8, Issue. 3, pp. 1-8, March. 2022.
[14] Edison Roberto C. Da Silva, Euzeli CiprianoDos Santos, Jr., and Cursino Bradao Jacobina, "Pulsewidth modulation strategies" *IEEE Ind. Electron., Magazine,* no.2, pp.37-45, June, 2011.
[15] Ahmet M. Hava, Russel J. Kerkman and Thomas A. Lipo, "A high-performance generalized discontinuous PWM algorithm" *IEEE Trans. Ind. Applicat.,* vol. 34, no. 5, Sep/Oct 1998, pp. 1059-1071.
[16] Olorunfemi Ojo, "The generalized discontinuous PWM scheme for three-phase voltage source inverters" *IEEE Trans. Ind. Electron.,* vol. 51, no. 6, Dec 2004, pp. 1280-1289.
[17] T. Brahmananda Reddy, J. Amarnath and D. Subbarayudu, "Direct torque control of induction motor based on Hybrid PWM method for reduced ripple: A sliding mode control approach" *ACSE Journal* Vol.6, Issue 4, Dec,2006, pp.23-30.
[18] Jose Rodriguez, Jih-Sheng Lai, Fang Zheng Peng: 'Multilevel Inverters: A Survey of Topologies, Control, and Applications', *IEEE Trans. On Ind. Elec.*, Vol. 49, No. 4, Aug. 2002.
[19] Abdul Rahiman Beig, G. Narayana, V.T. Ranganathan, "Modified SVPWM Algorithm for Three Level VSI With Synchronized and Symmetrical Waveforms", *IEEE Trans. Ind. Elect.*, Vol. 54, No. 1, Feb. 2007, pp 486-494.
[20] R.S. Kanchan, M.R. Baiju, K.K. Mohapatra, P.P. Ouseph and K. Gopakumar, "Space vector PWM signal generation for multilevel inverters using only the sampled amplitudes of reference phase voltages" *IEE Proc.-Electr. Power Appl*., vol. 152, No. 2, pp. 297-309, March 2005.
[21] S. Das and G. Narayanan, "Novel switching sequences for a space vector modulated three-level inverter," in *Proc. NPEC, IIT Roorkee*, Delhi, India, Jun. 2010.
[22] Soumitra Das and G. Narayanan, "Novel Switching Sequences for a Space-Vector-Modulated Three-Level Inverter", *IEEE Trans. Ind. Electron.,* vol. 59, no.3, Mar, 2012, pp. 1477-1487.
[23] Soumitra Das, G. Narayanan, and M. Pandey, "Space-Vector-Based Hybrid Pulsewidth ModulationTechniques for a Three Level Inverter", *IEEE Trans. Power Electron.,* vol. 29, no.9, Sep, 2014, pp. 4580-4591.
[24] Yi Deng, Koon Hoo Teo*,* Chunjie Duan*,* Thomas G. Habetler*,* and Ronald G. Harley*,* "A Fast and Generalized Space Vector Modulation Scheme for Multilevel Inverters", *IEEE Trans. Power Electron.,* vol. 29, no.10, Oct, 2014, pp. 5204-5217.
[25] Ui-Min Choi*,* June-Seok Lee*,* and Kyo-Beum Lee, "New Modulation Strategy to Balance the Neutral-Point Voltage for Three-Level Neutral-Clamped Inverter Systems", *IEEE Trans. Energy Conversion,* vol. 29, no.1, Mar, 2014, pp. 91-100
[26] Maramreddy Harshavardhan Reddy, Teegala .Bramhananda Reddy, "Discontinuous PWM Technique for the Asymmetrical Dual Inverter Configuration to Eliminate the Overcharging of DC Link Capacitor", IEEE Transactions on Industrial Electronics, Volume:65, Issue 1, Jan. 2018, pp. 156-166.
[27]. U. R. Muduli, B. Chikondra and R. K. Behera, "Novel Model Predictive DTC for Three-to-Five Phase Direct Matrix Converter Fed Induction Motor Drive," 2021 IEEE 12th Energy Conversion Congress & Exposition - Asia (ECCE-Asia), Singapore, Singapore, 2021, pp. 1505-1510, doi: 10.1109/ECCE-Asia49820.2021.9479067.

[28]. D. Vannurappa, G. P. R. Reddy, K. Deepak, Y. Hazarathaiah, S. S. Prasad and S. G. Malla, "Small Signal Analysis of Photovoltaic based Water-Pumping System Driven by Induction Motor," 2023 7th International Conference on Computing Methodologies and Communication (ICCMC), Erode, India, 2023, pp. 15-20, doi: 10.1109/ICCMC56507.2023.10083929.